Inclusive Scattering from Polarized ^{3}He and Neutron Form Factors

Haiyan Gao*

*Laboratory for Nuclear Science and Department of Physics[1]
Massachusetts Institute of Technology
Cambridge, Massachusetts 02139, U.S.A.

Abstract. Because of the lack of a free neutron target, deuterium targets had been used extensively in studying the neutron structure in the past from unpolarized electron-deuteron scattering experiments. Only recently polarized electron-deuteron scattering measurements have been performed which yield more precise information on the charge form factor of the neutron. The unique spin structure of the ^{3}He ground state and the recent developments in polarized target technologies make polarized ^{3}He targets very effective neutron targets. In this talk, I review the current status of the polarized ^{3}He targets and focus on the quasielastic asymmetry measurement from inclusive $^3\vec{H}e(\vec{e},e')$ process and the neutron form factors. I discuss the results of the MIT-Bates experiment 88-25 and the preliminary results of the recently completed JLab experiment E95-001 in which precision measurements of the neutron magnetic form factor at low Q^2 are aimed.

INTRODUCTION

Electromagnetic form factors are of fundamental importance for an understanding of the underlying structure of nucleons. Knowledge of the distribution of charge, magnetization within the nucleons provides a sensitive test of models based on Quantum Chromodynamics (QCD), as well as a basis for calculations of processes involving the electromagnetic interaction with complex nuclei. The understanding of the nucleon structure in terms of quark and gluon degrees of freedom of QCD will provide a basis to understand more complex strongly interacting matter at the level of quarks and gluons. While the proton form factors are known with excellent precision over a large range of four-momentum transfer Q^2, the corresponding data for the neutron are of inferior quality due to the lack of free neutron targets. Over the past decade, with the advent of improved experimental techniques, the precise determination of both the neutron electric form factor, G_E^n, and the magnetic

[1)] This work is supported in part by the U.S. Department of Energy under contract number DE-FC02-94ER40818.

form factor, G_M^n, has become a focus of experimental activity. While improving the precision of G_M^n is interesting in itself, it also benefits experiments designed to determine G_E^n, which usually measure the ratio G_E^n/G_M^n. Furthermore, precise data for the nucleon electromagnetic form factors are essential for the analysis of parity violation experiments designed to measure the strangeness content of the nucleon.

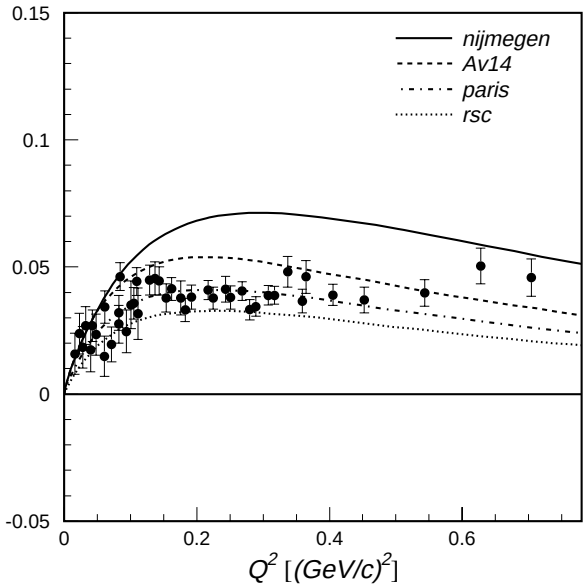

FIGURE 1. The electric form factor of the neutron as a function of four-momentum transfer from Platchkov *et al.* [1].

The most precise information on G_E^n at low Q^2 prior to any polarization experiment is from elastic electron-deuteron scattering experiment by Platchkov *et al.* [1]. However, the extracted G_E^n values are extremely sensitive to the deuteron structure. Fig. 1 shows the G_E^n values extracted with the Paris potential together with the fit of the data (dash-dotted curve). Fits from fitting the G_E^n data extracted with the Nijmegen potential, the Argonne V14 (AV14) and the Reid-Soft Core (RSC) NN potentials are shown as solid, dashed and dotted curves, respectively. The large spread represents the uncertainty of G_E^n due to the deuteron structure, and the absolute scale of G_E^n contains a systematic uncertainty of about 50% from the measurement by Platchkov *et al.* [1].

The development of polarized targets and beams has allowed more complete studies of electromagnetic structure than has been possible with unpolarized reactions. In quasielastic scattering, the spin degrees of freedom introduce new response functions into the differential cross section, thus providing additional information on nuclear structure [2]. Experiments with longitudinally polarized electron beams and recoil neutron polarimeters have been carried out at MIT-Bates [3] and Mainz [4,5] and G_E^n has been extracted from the $d(\vec{e},e'\vec{n})$ process. Recently, the neutron electric form factor was extracted for the first time [6] from $\vec{d}(\vec{e},e'n)$ reaction in which a vector polarized deuteron target from an atomic beam source was employed.

Using the polarization degrees of freedom, the proton contribution to the scattering process is suppressed and more precise information on the neutron charge form factor can be extracted. Currently, our best knowledge of G_E^n from these polarization measurements is $\sim 30\%$ for $Q^2 \leq 0.6(\mathrm{GeV/c})^2$.

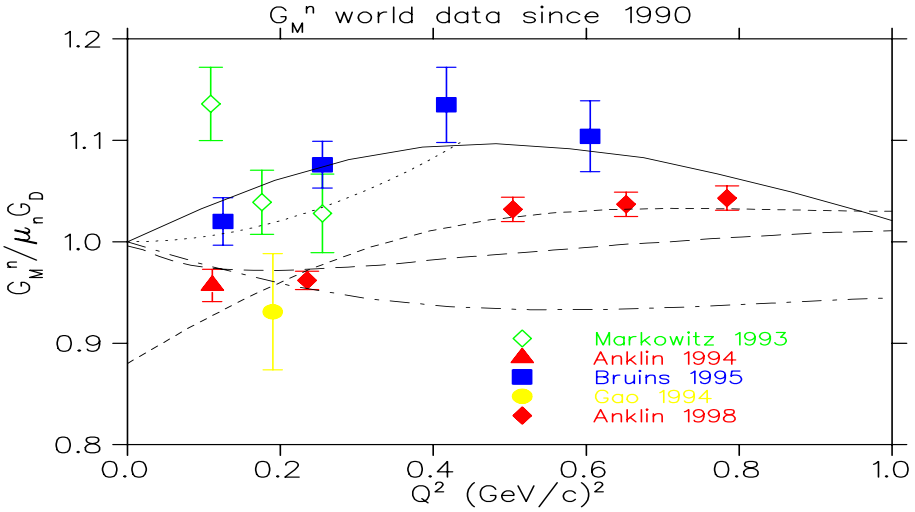

FIGURE 2. The neutron magnetic form factor G_M^n in units of the standard dipole parameterization, $\mu_n G_D$, in the low Q^2 region, as determined in several recent measurements: Markowitz *et al.* [7] (open diamonds) using $d(e,e'n)$; Anklin *et al.* [8] (triangle), Bruins *et al.* [9] (squares), and Anklin *et al.* [10] (solid diamonds) using the ratio $d(e,e'n)/d(e,e'p)$; and Gao *et al.* [11] (circle) using $^3\vec{\mathrm{H}}\mathrm{e}(\vec{e},e')$.

Until recently, most data on G_M^n had been deduced from elastic and quasielastic electron-deuteron scattering. For inclusive measurements, this procedure requires the subtraction of a large proton contribution and suffers from large theoretical uncertainties due to the deuteron model employed and corrections for final-state interactions (FSI) and meson-exchange currents (MEC), limiting the precision of G_M^n to $\sim$20% at low Q^2. The proton subtraction is avoided in coincidence $d(e,e'n)$ experiments [7], and the sensitivity to nuclear structure can be greatly reduced by measuring the cross section ratio $d(e,e'n)/d(e,e'p)$ in quasielastic kinematics. Several recent experiments [8–10] have employed the latter technique to extract G_M^n with uncertainties of $<2\%$ in the momentum transfer range $Q^2 = 0.1$ to 0.8 $(\mathrm{GeV/c})^2$. While this precision is excellent, the results of the experiments [7–10] are not fully consistent (cf. Figure 2). Furthermore, the two most precise data sets [9,10] of G_M^n seem to suggest a very different Q^2 dependence. In addition to the existing data, several theoretical calculations of G_M^n are shown in Figure 2. The solid curve

is an improved quark model calculation by Lu, Thomas and Williams [12] with a bag constant of 0.9 fm. The dotted curve is the minimal vector dominance model by Meissner [13]. The short and long dashed curves are the non-relativistic and relativistic quark model calculations by Eich [14] and Schlumpf [15], respectively. The dash-dotted line is a recent calculation by Mergell *et al.* [16] based on a fit of the proton data using dispersion theoretical arguments. These calculations clearly show very different behavior in the low Q^2 region. Thus, further data are desirable to clarify the situation with respect to the discrepancies among different measurements and theoretical calculations.

An alternative approach to a precision measurement of G_M^n is the inclusive quasielastic $^3\vec{\mathrm{He}}(\vec{e},e')$ process. In comparison to deuterium experiments, this technique employs a different target and relies on polarization degrees of freedom. It is thus subject to completely different systematics. A first such experiment was performed at the MIT-Bates [17] laboratory, and a result for G_M^n was extracted as shown in Figure 2.

The rest of the paper is organized as follows: Section II contains a discussion on the polarized ^{3}He target followed by Section III on the formalism for the spin-dependent inclusive quasielastic scattering, Section IV and V describe the MIT-Bates experiment 88-25 and JLab experiment E95-001, respectively.

I POLARIZED ^{3}HE TARGETS

Optical pumping technique is widely used to polarize a sample of atoms by transferring angular momentum from a pump light beam, typically a laser beam, to the sample atoms. In the case of ^{3}He, direct optical pumping between its ground state and the first excited state is not possible because of the energy difference involved. Metastability-exchange optical pumping and spin-exchange optical pumping are two indirect optical pumping techniques commonly used. In this section, I will review both techniques.

A Metastability-Exchange Optical Pumping

The metastability-exchange optical pumping technique was developed in the early 1960s at Rice university [18] to polarize ground state ^{3}He or ^{4}He atoms through metastability-exchange collisions with optically pumped ^{3}He or ^{4}He metastable atoms. This method involves optical pumping of 2^3S_1 metastable state atoms, then transferring the polarization to ^{3}He ground state atoms through metastability-exchange collisions, in which the excitation of the electronic cloud is exchanged leaving the ground state polarized after the collision.

Metastability-exchange optical pumping of ^{3}He works as following: metastable 2^3S_1 atoms are produced by an electrodeless weak radio frequency (RF) discharge in a glass cell filled to a pressure of order 1 torr of pure ^{3}He. The ratio of the ground

state atoms to the 2^3S_1 atoms is about 10^6 : 1; the exact number depends on discharge characteristics such as intensity, uniformity and the discharge frequency. The sample is placed in a weak uniform magnetic field which defines the spin direction of the sample. Right-handed or left-handed circularly polarized light (defined by the right-hand rule used in atomic physics) at $\lambda = 1083.4\ nm$ corresponding to the transition of $2^3S_1 \rightarrow 2^3P_0$ excites transitions between the 2^3S_1 and 2^3P_0 states with the selection rule $\Delta m = \pm 1$ depending on the helicity of the incident light (+ for the right-handed circularly polarized light and − for the left-handed case). The pumping light excites atoms from the $m_F = -\frac{1}{2}$ and $m_F = -\frac{3}{2}$ sublevels of the metastable state to the 2^3P_0 level which then decay back to all sublevels of 2^3S_1 through spontaneous emission. The result is that atoms from lower magnetic sublevels of the 2^3S_1 level ($m_F = -\frac{1}{2}$, $m_F = -\frac{3}{2}$) are transferred to higher sublevels of the 2^3S_1 level ($m_F = \frac{1}{2}$, $m_F = \frac{3}{2}$), hence the metastable atoms become polarized. In metastable state, hyperfine interaction mixes electronic polarization into nuclear polarization. The polarization of the metastable atoms is then transferred to the ground state through metastability-exchange collisions in which only the excitation of the electronic cloud is exchanged. If the ground state of ^{3}He is polarized, then the nucleus is polarized because the atom is in a $J = 0$ state. This process can be expressed schematically as:

$$^3He + {}^3\vec{H}e^* \rightarrow {}^3\vec{H}e + {}^3He^* \tag{1}$$

where $*$ denotes the 2^3S_1 metastable state and the vector notation indicates that the nucleus is polarized. This optical pumping technique only works for relatively low pressure conditions (0.1 torr to 10 torr). Destruction of metastables at the wall of the container dominates the relaxation at pressures below about 0.1 torr and at high pressures the lifetime of the metastable state atoms limits the optical pumping efficiency. It is also experimentally difficult to maintain a uniform discharge under high pressure conditions. Furthermore, it is necessary to operate optical pumping around room temperature to achieve efficient optical pumping because metastability exchange cross-section, σ_e, which is very temperature dependent for the case of ^{3}He atoms [19] [20]. σ_e decreases roughly two orders of magnitude between 300 K and 4.2 K. To make a relatively dense target for nuclear physics experiments, the compression and low temperature techniques have been used.

People have tried successfully to make a dense nuclear physics target by mechanically compressing the polarized gas. At Toronto, Timsit *et al.* in the early 1970s [21] constructed a dense target and achieved a density of $0.7 \times 10^{19}\text{cm}^{-3}$ with 3% polarization by compressing the gas with liquid mercury. However, the performance of these targets was severely limited by the absence of laser sources for optical pumping. At Mainz Otten *et al.* have designed and built a new type of dense polarized ^{3}He target using the compression method [22] [23] and have achieved pressures around 1 bar with 38% of polarization. Currently, such a target is operated at a pressure of $\sim$ 6.0 bar with a target polarization of $\sim$ 32% at an incident electron beam current of $\sim 10\mu$A [24].

Low temperature is another approach to take to construct a dense polarized ^{3}He target. A double-cell system consisting of a pumping cell and a target cell is a practical design for a polarized ^{3}He nuclear target. The pumping cell is at room temperature where metastability-exchange optical pumping can be performed efficiently and the target cell is cooled to low temperature where a practical luminosity can be achieved for a nuclear physics experiment. This idea was first explored at Rice University [25]. The ^{3}He nuclei in the target cell become polarized because the polarized ^{3}He atoms diffuse between the pumping cell and the target cell, reaching an equilibrium polarization state. External polarized ^{3}He targets based on this technique were employed in the MIT-Bates experiments [26] [17]. Optical measurement of the atomic polarization in the pumping cell provides a good monitor of the target nuclear polarization during the experiment. The atomic polarization and the nuclear polarization are related because of the hyperfine coupling and this indirect optical measurement of the ^{3}He nuclear polarization was calibrated carefully with the NMR technique at Caltech [27]. The metastability-exchange optical pumping technique has the unique features of pure atomic species and fast pumping rate for constructing an internal polarized ^{3}He target. The internal polarized ^{3}He targets based on this technique have been used successfully at IUCF, DESY and NIKHEF.

B Spin-Exchange Optical Pumping

In spin-exchange optical pumping, circularly polarized resonance light is absorbed by a saturated vapor of alkali-atoms contained in a glass cell. The cell also included a much larger quantity of noble-gas atoms. The spin angular momentum is transferred to the alkali-metal atoms, thereby spin-polarizing the valence electrons of the alkali-metal atoms. Subsequent spin-exchange collisions between the alkali-metal atoms and noble gas atoms transfer some of the electron-spin polarization to the nuclei of the noble gas.

Rubidium has been commonly used in polarized ^{3}He targets based on spin-exchange optical pumping technique. The high vapor pressure of rubidium allows operation at modest temperatures where chemical attack on the glass container is not a problem. The resonance line (794.7 nm corresponding to the transition between $5S_{1/2}$ and $5P_{1/2}$ levels) lies in a spectrum region where intense laser light is available from sources such as dye lasers, Ti:sapphire lasers, and more recently diode laser arrays.

A central feature of the target will be sealed glass target cells, which will contain a ^{3}He pressure of about 10 atmospheres. The cells will have two chambers, an upper chamber in which the spin exchange takes place, and a lower chamber, through which the electron beam will pass. In order to maintain the appropriate number density of alkali-metal (Rb) the upper chamber will be kept at a temperature of 170–200°C using an oven constructed of the high temperature plastic Torlon. A small amount of nitrogen gas is typically used in this type of target to quench the $P_{1/2}$ states, thus reducing the radiation trapping effect in order to reach high opti-

cal pumping efficiency. Radiation trapping occurs when the mean free path for the unpolarized photons is much shorter than the dimensions of the pumping vessel. The incident photons can be reemitted, i.e. resonantly scattered, and depolarized. Thus, additional dilution factor comes from the nitrogen present in the target. The dilution factor from the amount of rubidium in the target is typically negligible ($n_{Rb}/n_{He} \sim 10^{-4}$). Although the spin-exchange optical pumping technique is capable of producing a dense target (10 amagat), slow pumping time resulting from small spin-exchange cross section of ^{3}He atom and the Rb atom makes this technique only suitable for external polarized ^{3}He targets. NMR technique is typically used to measure the target polarization for this type of the targets. External polarized ^{3}He targets based on this technique have been used in experiments at JLab, MIT-Bates, SLAC and TRIUMF. Figure 3 shows the schematics of the spin-exchanged polarized ^{3}He target employed in electron scattering experiments in Hall A at Jefferson Laboratory (JLab) recently.

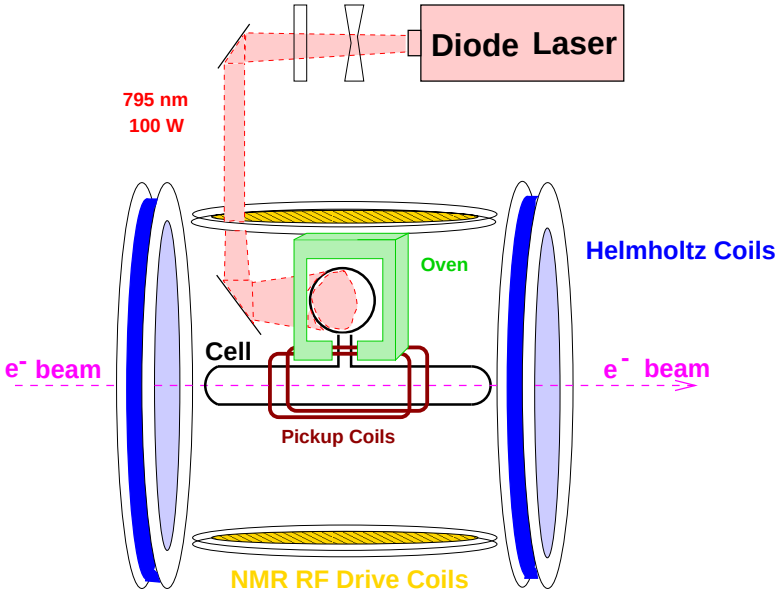

FIGURE 3. The schematics of the JLab Hall A polarized ^{3}He target based on the technique of the spin-exchange optical pumping.

II INCLUSIVE QUASIELASTIC SCATTERING OF POLARIZED ELECTRONS FROM POLARIZED ^{3}HE TARGETS

Polarized ^{3}He is a good candidate for an effective neutron target because its ground state wave function is dominated by the S-state in which the proton spins cancel and the nuclear spin is entirely due to the neutron. Therefore, inelastic scattering of polarized electrons from polarized ^{3}He in the vicinity of the quasielastic

peak should be useful for studying the neutron electromagnetic form factors.

The idea of using polarized ^{3}He nuclear target as an effective neutron target was first investigated by Blankleider and Woloshyn in closure approximation [28]. Friar *et al.* [29] have studied the model dependence in the spin structure of the ^{3}He wave function and its effect on the quasielastic asymmetry. The plane wave impulse approximation (PWIA) calculations performed independently by two groups [30,31] using spin-dependent spectral functions show that the spin-dependent asymmetries are very sensitive to the neutron electric or magnetic form factors at certain kinematics near the top of the quasielastic peak. Recently, Fadeev calculations have been carried out which include the final state interaction (FSI) [32], FSI and meson exchange current (MEC) [33]. These state-of-the-art three-body calculations are very important for extracting the neutron form factors from double polarization electron-^{3}He scattering experiments.

The differential cross section for the process $^3\vec{\mathrm{He}}(\vec{e},e')$ in the scattering plane can be written in terms of four nuclear response functions $R_K(Q^2,\nu)$ [2] as

$$\frac{d^2\sigma}{d\Omega dE'} = \sigma_{Mott}\left[v_L R_L + v_T R_T - h(\cos\theta^* v_{T'} R_{T'} + 2\sin\theta^*\cos\phi^* v_{TL'} R_{TL'})\right], \quad (2)$$

where θ^* and ϕ^* are the polar and azimuthal angles defining the direction of the target spin with respect to the momentum transfer vector $\vec{q}$ the v_K are kinematic factors, ν is the electron energy loss, h is the helicity of the incident electron, and $Q^2 \equiv \vec{q}^{\,2} - \nu^2$. $R_{T'}$ and $R_{TL'}$ are two response functions arising from the polarization degrees of freedom. An experimentally clean signature of these observables is the spin-dependent asymmetry, defined as

$$A = \frac{\sigma_+ - \sigma_-}{\sigma_+ + \sigma_-} = -\frac{\cos\theta^* v_{T'} R_{T'} + 2\sin\theta^*\cos\phi^* v_{TL'} R_{TL'}}{v_T R_T + v_L R_L}, \quad (3)$$

where the subscript $+$ $(-)$ refers to the electron helicity h. By orienting the target spin at $\theta^* = 0^\circ$ or $\theta^* = 90^\circ$, corresponding to the spin direction either along the 3-momentum transfer vector $\vec{q}$ or normal to it, one can select the transverse asymmetry $A_{T'}$ (proportional to $R_{T'}$) or the transverse-longitudinal asymmetry $A_{TL'}$ (proportional to $R_{TL'}$).

In plane wave impulse approximation (PWIA) the cross section for $^3\vec{\mathrm{He}}(\vec{e},e')$ at the center of the quasielastic peak is (roughly) proportional to the sum of the en plus twice the ep elastic cross section. The cross section for polarized electron-nucleon scattering is

$$\frac{d\sigma_{eN}}{d\Omega} = \sigma_{Mott}\frac{E'}{E}\Big[v_L(1+\tau)G_E^2 + v_{TL'}2\tau G_M^2 - h\,\bar{p}_N(\cos\theta^* v_{T'}2\tau G_M^2 - 2\sin\theta^*\cos\phi^* v_{TL'}\sqrt{2\tau(1+\tau)}G_M G_E)\Big], \quad (4)$$

where $\tau = Q^2/(4M^2)$, and $\bar{p}_N$ is the effective nucleon polarization. As a consequence of the S-state dominance, the neutron in ^{3}He is almost fully polarized,

$\bar{p}_n \approx 1$, at the quasielastic peak while the remaining small components of the ^{3}He ground state, the D state ($\sim$8%) and the mixed-symmetry S' state ($\sim$1%), give rise to a small net proton polarization of $\bar{p}_p \approx -0.03$ [29]. Combining the above equations, the transverse asymmetry can be written

$$A_{T'} \propto \frac{\sigma_n}{(\sigma_n + 2\sigma_p)} \bar{p}_n (G_M^n)^2 + \frac{2\sigma_p}{(\sigma_n + 2\sigma_p)} \bar{p}_p (G_M^p)^2, \tag{5}$$

where σ_n and σ_p are the electron-neutron and electron-proton elastic scattering cross sections, respectively. Since G_M^n and G_M^p are comparable in magnitude, but $|\bar{p}_p| \ll |\bar{p}_n|$, $A_{T'}$ is dominated by the neutron contribution and so is essentially proportional to $(G_M^n)^2$. Note that it is mostly the proton contribution that is sensitive to details of the ^{3}He ground state wave function.

The strong sensitivity of $A_{T'}$ to $(G_M^n)^2$ in quasielastic kinematics has been verified in a number of recent calculations [30–33]. The most advanced of these include corrections for FSI [32] and FSI and MEC [33], which are relatively small at the quasielastic peak. One may conclude that $A_{T'}$ depends only weakly on the details of the ^{3}He nuclear ground state and the reaction mechanism. Thus, a precision measurement of $A_{T'}$ is suitable to extract precise information on G_M^n.

While $A_{TL'}$ is sensitive to the product of G_E^n and G_M^n, a dominant proton contribution to $A_{TL'}$ greatly reduces the sensitivity to G_E^n at low Q^2 from inclusive $^3\vec{H}e(\vec{e}, e')$ process.

III MIT-BATES EXPERIMENT 88-25

The experiment was performed at the MIT-Bates Linear Accelerator Center in spring 1993 using a 370 MeV longitudinally polarized electron beam. A Wien spin rotator was employed to produce longitudinally polarized electrons at the target. The average beam current during the experiment was 25 μA and the average beam polarization was determined using a Møller apparatus [34] to be 36.5%.

The polarized ^{3}He target used in this experiment was a double-cell system consisting of a glass pumping cell and a copper target cell. The target was polarized by the metastability-exchange optical pumping technique [35]. The target was operated at 13 K during the experiment with a ^{3}He gas pressure of 2.2 torr. The target wall was coated with a thin layer of nitrogen to maintain a sufficiently long relaxation time at low temperature. A holding field of 36 gauss provided by a pair of Helmholtz coils defined the target spin quantization axis. The target spin direction was aligned at an angle of 42.5° to the electron beam. The pumping cell polarization was measured continuously by monitoring the circular polarization of the 668-nm line excited by the ^{3}He discharge. The target polarization was inferred from the polarization of the pumping cell and the time constants of the coupled system. This optical measurement of the ^{3}He nuclear polarization was calibrated by an NMR measurement [27] with an accuracy of $\pm$2%. With 25μA of beam, the target polarization was 38% or greater.

The scattered electrons were detected in the Medium Energy Pion Spectrometer (MEPS) and the One Hundred Inch Spectrometer (OHIPS) configured at an electron scattering angle $\theta = 91.4°$ to the left of the beam and 70.1° to the right of the beam, respectively. The MEPS spectrometer central momentum was 250 MeV/c corresponding to $Q^2 = 0.19$ (GeV/c)^2 and $\theta^* = 8.9°$ or 171.1° for positive or negative target polarization, respectively. The OHIPS spectrometer had a central momentum of 285 MeV/c, corresponding to the QE kinematic setting for $A_{TL'}$ measurement at a $Q^2 = 0.14$ (GeV/c)^2. While the MEPS detector package consisted of two vertical drift chambers, three planes of trigger hodoscopes, and an Aerogel Čerenkov detector, the OHIPS detector package consisted of two crossed drift chambers, three planes of plastic scintillators, and an isobutane gas Čerenkov detector. The triggers were formed by events for which all three hodoscopes fired in each spectrometer. The Čerenkov detectors were used for pion rejection.

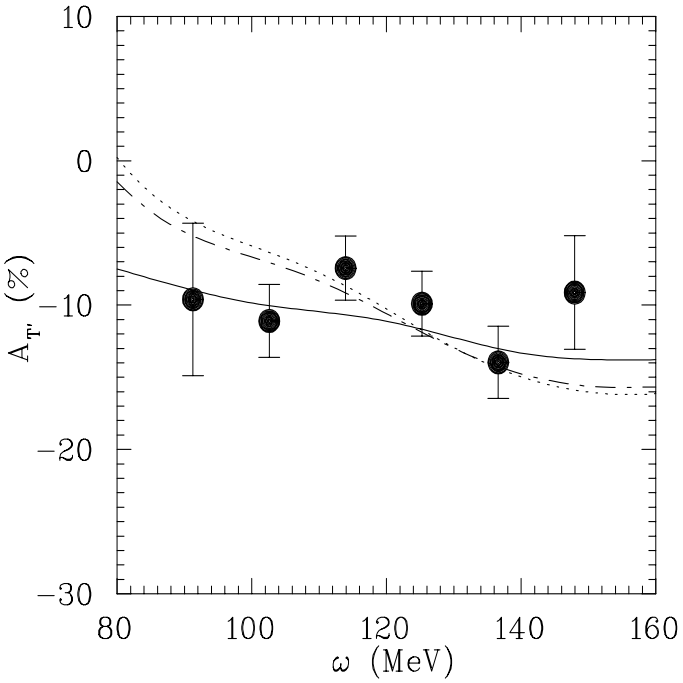

FIGURE 4. Transverse asymmetry $A_{T'}$ from the MIT-Bates experiment 88-25 [17] as a function of electron energy loss ω. The data are shown with statistical uncertainties only. The solid line is the calculation by Ishikawa *et al.*. The dashed line is the calculation by Salm'e *et al.* and the dash-dotted line is the calculation by Schulze *et al.*.

Fig. 4 shows the measured ^{3}He inclusive spin-dependent quasielastic transverse asymmetry $A_{T'}$ [17], as a function of the electron energy transfer, ω, together with the two PWIA calculations and the calculation by Ishikawa *et al.* [32]. The deviation of the result by Ishikawa *et al.* from those of PWIA calculations [30] [31] is significant away from the quasielastic peak. The agreement between the data on $A_{T'}(\omega)$ and the calculation by Ishikawa *et al.* is excellent in terms of the magnitude of the asymmetry and also the shape. Unfortunately, because of

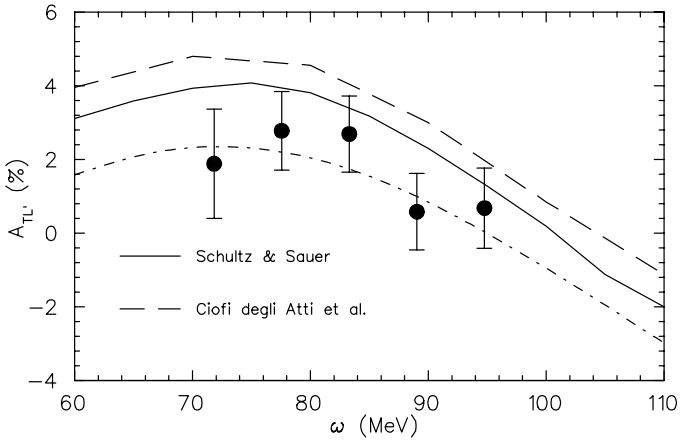

FIGURE 5. Longitudinal-transverse asymmetry $A_{TL'}$ from MIT-Bates experiment [17] as a function of electron energy loss ω. The data are shown with statistical uncertainties only. The solid line is the calculation by Ishikawa *et al.*. The dashed line is the calculation by Salmé *et al.* and the dash-dotted line is the calculation by Schulze *et al.*.

the large errors associated with the measured $A_{T'}(\omega)$ as shown in Fig. 4, it is not possible to put constraints on the theoretical calculations of the ^{3}He inclusive spin-dependent quasielastic asymmetry.

Because of the limitation of the statistics of this measurement, the measured quasielastic asymmetry, $A_{T'}(\omega)$, averaged over the experimental ω acceptance was used in extracting ${G_M^n}^2$ together with the calculation of Ishikawa *et al.* [32]. The G_M^n value extracted from this experiment at $Q^2 = 0.19$ (GeV/c)^2 is shown (Fig. 3, closed circle) with total uncertainty dominated by the statistical uncertainty.

On the other hand, $A_{TL'}$ from quasielastic $^3\vec{H}e(\vec{e},e')$ at low Q^2 is ($Q^2 \leq 0.3\ (GeV/c)^2$) is dominated by the proton contribution largely because of the smallness of ${G_E^n}^2$ and the small non-S state part of the ^{3}He ground state wave function. Thus, it is questionable to extract information on G_E^n at low Q^2 from $^3\vec{H}e(\vec{e},e')$. It is possible to go to higher Q^2 ($Q^2 \geq 0.3(GeV/c)^2$) to extract ${G_E^n}^2$ with respectable accuracy from quasielastic $^3\vec{H}e(\vec{e},e')$ measurement where the proton contribution to $A_{TL'}$ is under better control. Fig. 5 shows $A_{TL'}$ from the MIT-Bates experiment [17] as a function of ω together with the PWIA calculations and the calculation by Ishikawa *et al.* [32] which included FSI. The PWIA calculations are consistently higher than the measured asymmetry. The calculation with FSI is in better agreement with the data.

To extract precise information on G_M^n from inclusive quasielastic $A_{T'}$ measurement, it is important to measure $A_{T'}$ with high precision across the ^3He quasielastic peak. As away from the quasielastic peak, predictions from different models deviate. Thus, one can constrain theoretical model using high precision data of $A_{T'}$ in the wings of the QE peak. To extract precise information on G_M^n, one then use the measured $A_{T'}$ right on top of the quasielastic peak, this is a procedure much less sensitive to model dependence than the procedure used in extracting G_M^n from the

MIT-Bates experiment 88-25.

IV JLAB EXPERIMENT E95-001

The experiment was carried out in Hall A at JLab in early 1999 using a longitudinally polarized CW electron beam at energies of 0.778 and 1.727 GeV and 10 μA of beam current. A high pressure ^{3}He gas target was polarized via spin-exchange optical pumping at a density of 2.5×10^{20} nuclei/cm^3. The effective target length seen by the spectrometers was 10 cm/sin θ_e, where θ_e is the electron scattering angle. To facilitate optical pumping, the target contained small admixtures of nitrogen ($\sim 10^{18}$ cm^{-3}) and rubidium ($\sim 10^{14}$ cm^{-3}). Background from the nitrogen was determined in calibration measurements using a reference cell which has the same dimensions as those of the ^{3}He target cell and is corrected for in the analysis; the contribution from rubidium is negligible. The beam and target polarizations were approximately 70% and 30%, respectively. The beam helicity was reversed randomly at a rate of 1 Hz. A total beam charge of approximately 22 C was accumulated, resulting in a total data set of 1.3×10^9 quasielastic events after background subtraction.

Six kinematic points were measured corresponding to $Q^2 = 0.1$ to 0.6 (GeV/c)^2 in steps of 0.1 (GeV/c)^2. To maximize sensitivity to $A_{T'}$, the target spin was oriented at -62.5° with respect to the beam direction, resulting in a contribution to the asymmetry due to $R_{TL'}$ of less than 2% for all kinematic points. The target spin direction was rotated by 180° every 24-48 hours for systematic checks, causing the asymmetry to change sign. The beam helicity definition was also reversed every 24 hours for systematic checks associated with the electron beam helicity. The scattered electrons were observed in the two Hall A High Resolution Spectrometers, HRSe and HRSh. Both spectrometers were configured to detect electrons in single-arm mode using nearly identical detector packages consisting of two dual-plane vertical drift chambers for tracking, two planes of segmented plastic scintillators for trigger formation, and a CO_2 gas Cherenkov detector and Pb-glass total-absorption shower counter for particle identification. Pion background was rejected using the Cherenkov and shower counter information. The spectrometer momentum and angular acceptances were approximately $\pm 4.5\%$ and 5.5 msr, respectively. The level of background from the walls of the glass target was measured at regular intervals with the target cell empty and was less than about 5% of the full target yield. The HRSe was set for quasielastic kinematics while the HRSh detected elastically scattered electrons. The elastic asymmetry can be calculated to better than 2% using the well-known elastic form factors of ^{3}He [36], and so the elastic measurement allows precise monitoring of the product of beam and target polarizations. Standard Møller and NMR polarimetry was also performed and served as a cross-check.

A statistical precision in $A_{T'}$ of $\sim$ 2.0% was achieved for each Q^2 point in a ± 15 MeV bin around the center of the quasielastic peak. Fig. 6 shows the preliminary E95-001 result of $A_{T'}$ with statistical errors as a function of ω at $Q^2 = 0.1$

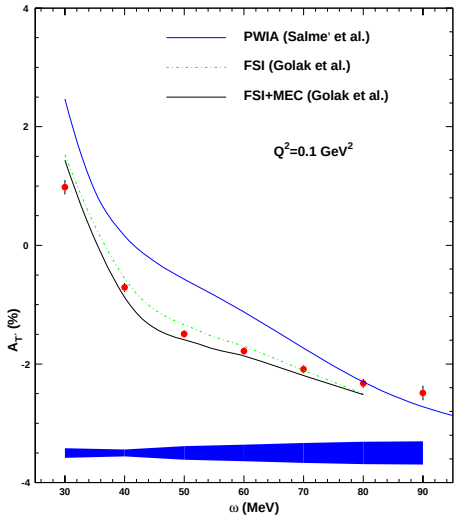

FIGURE 6. The preliminary E95-001 $A_{T'}$ result as a function of ω at $Q^2 = 0.1$ (GeV/c)^2.

(GeV/c)^2 together with the PWIA calculation of Ref. [31] and calculations with FSI and FSI+MEC by Golak *et al.* [33]. The error band shows the preliminary systematic uncertainty of the measurement, which will be reduced to a level comparable to the statistical uncertainty of the measurement after detailed analysis. This precision is better by about a factor of five that that of our previous experiment on ^{3}He [17] at $Q^2 = 0.19$ (GeV/c)^2. Extraction of G_M^n from the data requires the use of theoretical calculations. Currently the Bochum-Krakow group [33] is carrying out extensive calculations of $A_{T'}$ as a function of G_M^n for the kinematics of this experiment which include the FSI and MEC effects. This is the state-of-the-art three-body calculation. In addition, an independent calculation of the ^{3}He quasielastic asymmetry which will include FSI and MEC effects is currently in progress [37]. The Bochum-Krakow calculation will be convoluted with the experi-

mental acceptances, and G_M^n will be determined using a best fit of $A_{T'}(G_M^n)$ to the data in the vicinity of the quasielastic peak. Fig. 7 shows the expected precision for G_M^n from this experiment. The data also allow a detailed analysis of the dependence of $A_{T'}$ on the electron energy transfer ω. The regions away from the quasielastic peak are expected to be sensitive to details of the reaction mechanism. Thus, the shape of $A_{T'}(\nu)$ can be used to constrain calculations that include FSI and MEC corrections. Data analysis is currently in progress and results are expected in late 1999.

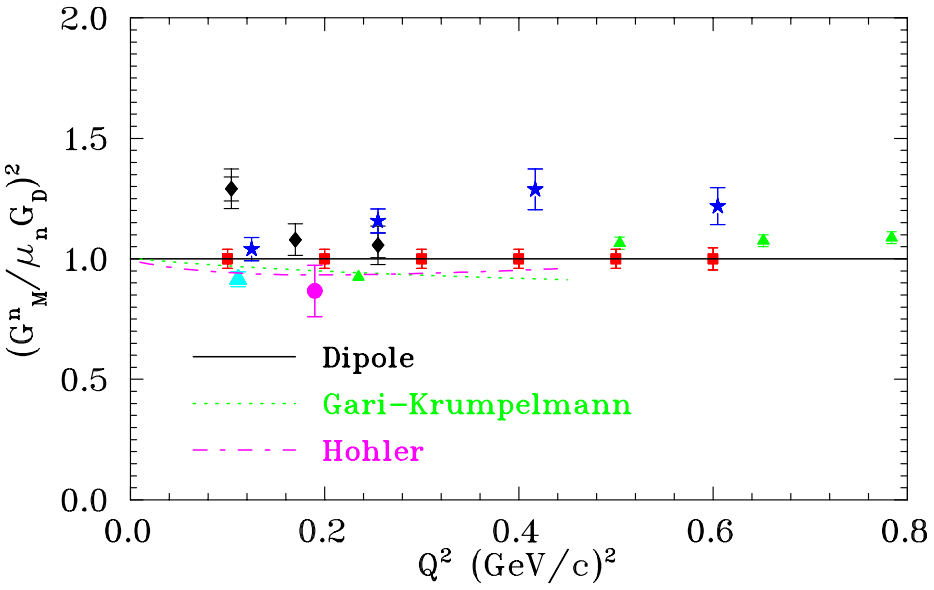

FIGURE 7. The neutron magnetic form factor ${G_M^n}^2$ in units of the standard dipole parameterization, $(\mu_n G_D)^2$, in the low Q^2 region, as determined in several recent measurements. The projected results from the JLab experiment (E95-001) are shown as solid squares using the $^3\vec{\mathrm{He}}(\vec{e},e')$ process.

REFERENCES

1. S. Platchkov *et al.*, Nucl. Phys. **A510**, 740 (1990).
2. T.W. Donnelly and A.S. Raskin, Ann. Phys. (N.Y.) **169** (1986) 247.

3. T. Eden *et al.*, Phys. Rev. **C50**, R1749 (1994).
4. M. Ostrick *et al.*, Phys. Rev. Lett. **83**, 276 (1999).
5. C. Herberg *et al.*, Eur. Phys. Jour. **A5**, 131 (1999).
6. I. Passchier *et al.*, Phys. Rev. Lett. **82**, 4988 (1999).
7. P. Markowitz *et al.*, Phys. Rev. **C48** (1993) R5.
8. H. Anklin *et al.*, Phys. Lett. **B336** (1994) 313.
9. E.E.W. Bruins *et al.*, Phys. Rev. Lett. **75** (1995) 21.
10. H. Anklin *et al.*, Phys. Lett. **B428** (1998) 248.
11. H. Gao *et al.*, Phys. Rev. **C50** (1994) R546.
12. D.H. Lu, A.W. Thomas, A.G. Williams, Phys. Rev. **C57**, 2628 (1998).
13. U.-G. Meissner, Phys. Rep. **161**, 213 (1988).
14. E. Eich, Z. Phys. **C45**, 627 (1988).
15. F. Schlumpf, J. Phys. **G20** 237, 1994.
16. P. Mergell, U.-G. Meissner, D. Dreshel, Nucl. Phys. **A 596**, 367 (1996).
17. H. Gao *et al.*, Phys. Rev. **C50**, R546 (1994); H. Gao, Ph.D. thesis, California Institute of Technology (unpublished, 1994); J.-O. Hansen *et al.*, Phys. Rev. Lett. **74**, 654 (1995).
18. F.D. Colegrove, L.D. Shearer, and G.K. Walters, Phys. Rev. Lett. **132**, 2561 (1963).
19. P.J. Nacher and M. Leduc, J. Phys. **46**, 2057 (1985).
20. F.D. Colegrove, L.D. Shearer, and G.K. Walters, Phys. Rev. **135**, A353 (1964).
21. R.S. Timsit *et al.*, Can. J. Phys. **49**, 509 (1971).
22. G. Eckert, W. Heil *et al.*, Nucl. Inst. Meth. **A320**, 53 (1992).
23. M. Meyerhoff *et al.*, Doctoral thesis, Mainz University (1994).
24. R. Surkau *et al.*, Nucl. Instrum. Methods Phys. Res. Sect. A**384**, 444 (1997).
25. H.H. Mc Adams, Phys. Rev. **170**, 276 (1968). **A47**, 468 (1993).
26. C.E. Woodward *et al.*, Phys. Rev. Lett. **65**, 698 (1990).
27. W. Lorenzon, T.R. Gentile, H. Gao, and R.D. McKeown, Phys. Rev.
28. B. Blankleider and R.M. Woloshyn, Phys. Rev. **C29**, 538 (1984).
29. J.L. Friar *et al.*, Phys. Rev. **C42** (1990) 2310.
30. R.-W. Schulze and P.U. Sauer, Phys. Rev. **C48** (1993) 38.
31. C. Ciofi degli Atti, E. Pace and G. Salmè, Phys. Rev. **C51** (1995) 1108; C. Ciofi degli Atti, E. Pace and G. Salmè, in *Proceedings of the 6th Workshop on Perspectives in Nuclear Physics at Intermediate Energies*, ICTP, Trieste May 1993, (World Scientific); C. Ciofi degli Atti, E. Pace and G. Salmè, Phys. Rev. **C51**, 1108 (1995); G. Salmè, private communication.
32. S. Ishikawa *et al.*, Phys. Rev. **C57** (1998) 39; and private communication.
33. J. Golak, private communication.
34. J. Arrington, E.J. Beise, B.W. Filippone, T.G. O'Neill, W.R. Dodge, G.W. Dodson, K.A. Dow, and J.D. Zumbro, Nuclear Instrument and Methods **A311**, 39 (1992).
35. R.G. Milner, R.D. McKeown, and C.E. Woodward, Nucl. Instrum. Methods Phys. Res., Sec. **A274**, 56 (1989); C.E. Jones *et al.*, Phys. Rev. **C47**, 110 (1993).
36. A. Amroun *et al.*, Nucl. Phys. **A579** (1994) 596.
37. G. Salmé, private communication.